

Advancing drag crisis of a sphere via the manipulation of integral length scale

Niloofer Moradian^{1a}, David S-K. Ting^{1b} and Shaohong Cheng^{*2c}

¹*Department of Mechanical, Automotive and Materials Engineering, University of Windsor,
401 Sunset Avenue, Windsor, ON, Canada N9B 3P4*

²*Department of Civil and Environmental Engineering, University of Windsor,
401 Sunset Avenue, Windsor, ON, Canada N9B 3P4*

(Received July 16, 2009, Accepted May 19, 2010)

Abstract. Spherical object in wind is a common scenario in daily life and engineering practice. The main challenge in understanding the aerodynamics in turbulent wind lies in the multi-aspect of turbulence. This paper presents a wind tunnel study, which focuses on the role of turbulence integral length scale Λ on the drag of a sphere. Particular turbulent flow conditions were achieved via the proper combination of wind speed, orifice perforated plate, sphere diameter (D) and distance downstream from the plate. The drag was measured in turbulent flow with $2.2 \times 10^4 \leq Re \leq 8 \times 10^4$, $0.043 \leq \Lambda/D \leq 3.24$, and turbulence intensity Tu up to 6.3%. Our results confirmed the general trends of decreasing drag coefficient and critical Reynolds number with increasing turbulence intensity. More interestingly, the unique role of the relative integral length scale has been revealed. Over the range of conditions studied, an integral length of approximately 65% the sphere diameter is most effective in reducing the drag.

Keywords: sphere; orifice perforated plate; turbulence; drag coefficient; integral length scale.

1. Introduction

Lowering the drag associated with a bluff body such as a sphere is of both fundamental and practical importance. For example, when designing a golf ball, dimples are created on its surface to lower the Reynolds number at which the drag crisis occurs, enabling it to travel a longer distance compared to its smooth surface counterpart. It is now known that the standardized dimple design has not been optimized to give the golf ball the best aerodynamic performance. This appears to be partially due to the fact that wind turbulence has not been carefully considered in the classical design. The omnipresent turbulence can significantly alter the aerodynamics of a sphere in an otherwise laminar flow stream.

Extensive research efforts have been dedicated to understand the aerodynamics of a smooth sphere in no turbulent (or smooth) flow conditions. Fig. 1 portrays a collection of experimental and

* Corresponding Author, Associate Professor, E-mail: shaohong@uwindsor.ca
a Graduate Student

b Professor

c Associate Professor

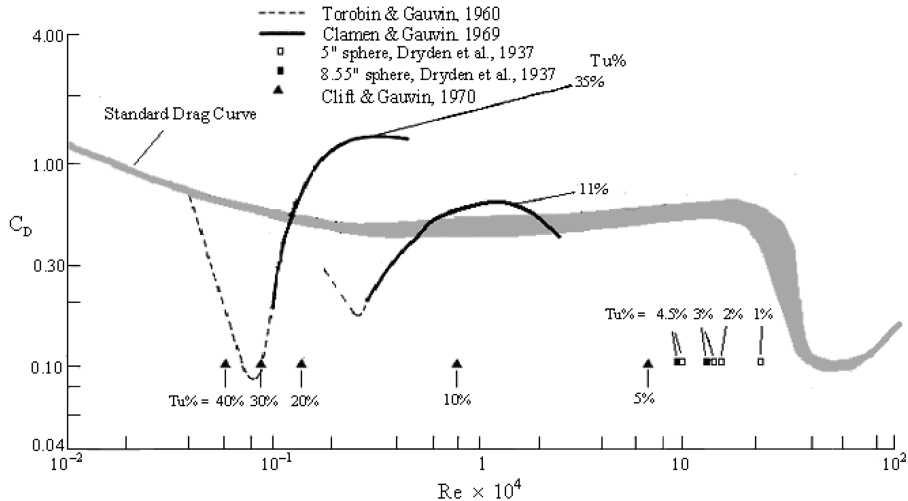


Fig. 1 Drag coefficient of sphere as a function of Reynolds number for different Tu

numerical data from existing literatures (Shepherd and Lapple 1940, Torobin and Gauvin 1959, Clift and Gauvin 1970, 1971, Achenbach 1972, Schlichting 1979), of which the relation between drag coefficient C_D and Reynolds number Re in smooth flow condition is shown by the shaded band. This shall be referred to as the standard C_D - Re curve in the current paper. The flow pattern around a sphere, particularly in the wake region, varies with the Reynolds number. For $10^3 < Re < 10^5$, which covers the Reynolds number range of 2.2×10^4 to 8×10^4 considered in the present study, the vortex loop shedding becomes nearly a continuous process (Lamb 1945). Flow visualization (Bakic and Peric 2005) shows that the far wake region continues to grow in size and produces a wave-like motion. Fig. 1 shows that the value of C_D virtually remains constant in this regime. As we approach the critical Reynolds number, $Re_{cr} \approx 3.5 \times 10^5$, the boundary layer around the sphere transits from laminar to turbulent, leading to the increased momentum near the boundary and the delay in flow separation (Çengel and Cimbala 2006). The wake region becomes narrower, resulting in a sudden reduction in the drag coefficient (Schlichting 1955).

As most flows encountered in practice and in nature are turbulent flows, the influence of flow turbulence on sphere aerodynamics has been the subject of numerous wind tunnel studies (e.g., Dryden and Kuethe 1930, Ahlbom 1931, Dryden *et al.* 1937, Brownlee 1960, Torobin and Gauvin 1960, Clamen and Gauvin 1969, Clift and Gauvin 1970, Anderson and Uhlherr 1977, Sankagiri and Ruff 1997, Mohd-Yusof 1996). The consensus of these experimental studies is that an increase in turbulence intensity would reduce the value of Reynolds number for boundary layer flow transition. In other words, the value of the critical Reynolds number, Re_{cr} is very sensitive to free-stream turbulence. This finding supports Prandtl's (1914) suggestion that such resistance curves of sphere can be used to compare the flow characteristics in different wind tunnels; in particular, with respect to their lesser or greater turbulence. However, most of these past studies only focused on the effect of turbulence intensity on sphere aerodynamics. For example, Dryden *et al.* (1937) pointed out that for turbulent flow over a stationary sphere, turbulence intensity was the most important turbulent parameter that affects the critical Reynolds number. The value of Re_{cr} was decreased from 3.5×10^5 in smooth flow condition to around 10^5 when the turbulence intensity was increased to 4.5%. Torobin and Gauvin (1960, 1961) and subsequently, Clamen and Gauvin (1969) measured drag on

moving spherical bodies. A grid system was used to generate turbulence in the wind tunnel. Spherical objects of different sizes were injected upstream of the tunnel to have velocities close to that of the oncoming air stream. It was found that the C_D -Re curves corresponding to different turbulence intensity levels had similar shapes except that the minimum-maximum C_D occurred at different Reynolds numbers. When increasing Re beyond Re_{cr} , the drag coefficient of their moving spheres first increased and then decreased. They speculated that the increase in C_D , right after its dip at Re_{cr} , could be due to the occurrence of super turbulent flow regime. In more intense turbulent flow, the magnitude of the maximum C_D tended to be greater, whereas the corresponding Reynolds number was smaller. In addition, Clift and Gauvin (1970) numerically studied stationary and moving spherical particles in turbulent flow. By defining an equation to predict the value of critical Reynolds number associated with flow of different turbulence intensities, it was shown that the critical Reynolds number decreases with increasing turbulence intensity. Results from these studies are also presented in Fig. 1. A more recent moving sphere drag measurement by Sankagiri and Ruff (1997) in high turbulence intensity flow (Tu more than 30%) covered the sub-critical, critical, and super-critical Reynolds number regions. In the sub-critical range, the drag was found to be greater than the standard one with a gradual decrease into the critical regime. The behavior at the critical and super-critical Reynolds numbers agreed fairly well with previous study by Clift and Gauvin (1971).

When studying aerodynamics of a bluff body in turbulent flow, it is important to appreciate the complicated multi-aspect nature of turbulence; i.e., other than the turbulence intensity, the integral length scale, which represents the size of the energy containing eddies, is yet another parameter of great significance in defining the flow condition. A change in turbulence intensity typically leads to associated variations in the turbulent length scale. Nevertheless, only a few researchers noted the possible role played by the integral length scale when altering turbulence intensity in their studies. Torobin and Gauvin (1961) varied the relative integral length scale Λ/D (where D is the sphere diameter) from 2 to 6.25 for $500 < Re < 2100$, but failed to detect a definite role of Λ/D in the C_D -Re relationship. For lower Reynolds numbers, $200 < Re < 800$, Zarin (1970) and Zarin and Nicholls (1971) found that for turbulent wind over a fixed sphere, where the integral length scales were an order of magnitude larger than the sphere diameter, the drag increased with increasing Tu from 0.4% to 3.3%. They also reported a monotonically decreasing C_D with increasing sphere diameter over $600 \leq Re \leq 5000$, and $0.16 \leq \Lambda/D \leq 2$. Neve (1986) and Neve and Shansonga (1989) studied sphere drag of a fixed 37.7 mm diameter sphere for $5 \times 10^3 < Re < 10^5$, $Tu < 25\%$ and $\Lambda/D < 5$. While no specific conclusion regarding the relative integral length effect was reached, their results showed that at certain combination of turbulence intensity and relative integral length scale, the drag coefficient could be reduced to less than 0.15; see Fig. 2.

It is clear from the literature review that there is a qualitative consensus concerning the effect of turbulence intensity on the C_D -Re relationship of a sphere in turbulent flow. Quantitatively, however, the discrepancies among different studies are overwhelming. The main factor contributing to these discrepancies is probably Λ , which has neither been measured nor controlled in most studies. This integral length which is coupled with Tu, can significantly affect C_D under some conditions. Therefore, an attempt is made to assimilate the turbulent wind by quasi-independently controlling the energy containing integral length scale, in addition to the turbulence intensity and Reynolds number. Specifically, this study aims at uncovering the independent role of relative integral length scale Λ/D on the drag of a sphere when approaching the critical Reynolds number range. The preliminary results obtained by using three stationary PVC spheres in a wind tunnel over a Reynolds number range from 2.2×10^4 to 8×10^4 , turbulence intensity up to 10.7%, and relative

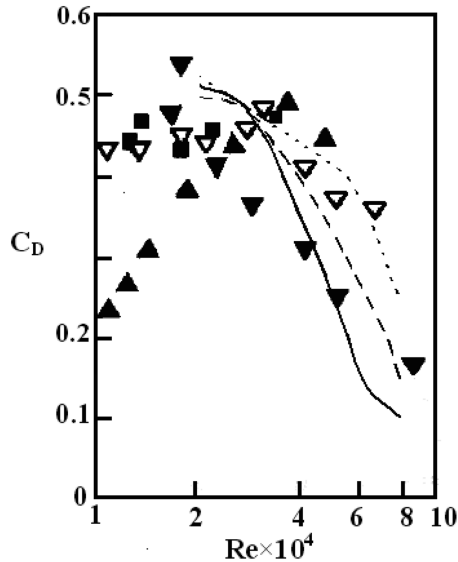


Fig. 2 The effect of relative integral length scale on drag coefficient:

▼ Tu = 10%, (Λ/D) = 0.08, Neve (1986); ▽ Tu = 10%, (Λ/D) = 0.5, Neve and Shansonga (1989); ■ Tu = 10%, (Λ/D) = 0.8, Neve (1986), Neve and Shansonga (1989); ▲ Tu = 10%, (Λ/D) = 1.5, Neve (1986), Neve and Shansonga (1989); ··· Tu = 2.5%, (Λ/D) = 0.63, Moradian *et al.* (2009); — Tu = 4%, (Λ/D) = 0.67, Moradian *et al.* (2009); — Tu = 6.3%, (Λ/D) = 0.7, Moradian *et al.* (2009)

integral length scale Λ/D of 0.1 to 2.6, have been reported in Moradian *et al.* (2009).

2. Experimental details

2.1 Turbulence generation

The experiments were conducted in a low-speed, closed-loop wind tunnel at the University of Windsor. The 4 m long test section is 0.75 m by 0.75 m at the inlet and expands to 0.765 m \times 0.765 m at the outlet to accommodate boundary layer built up. The maximum attainable velocity of the wind tunnel is around 20 m/s. The background turbulence level is found to be less than 0.3%.

Three 6 mm thick orifice perforated aluminum plates were used to simulate different turbulent flow conditions. The turbulence was generated by placing one of the three plates near the inlet of the wind tunnel. As sketched in Figs. 3(a) to 3(c), the hole diameter d of the plates were 25 mm, 37.5 mm and 50 mm, respectively. The solidity ratio of all three plates was kept the same at 43%. To minimize the impact of the plate thickness on the generated turbulent flow field, each hole was machined into an orifice with a 41° angle, as illustrated in Fig. 3(d). The same turbulence generation mechanism was adopted by Liu and Ting (2007) and Liu *et al.* (2007), of which it was concluded that an orifice perforated plate of 6 mm thickness, 41° orifice angle, and 43% solidity ratio was appropriate for generating clean, simple, quasi-isotropic turbulence. The flow field was found to be uniform in terms of mean flow velocity, turbulence intensity and integral length scale in the core region of the testing cross section.

For quantifying flow velocities and the associated turbulent parameters, a hot-wire system

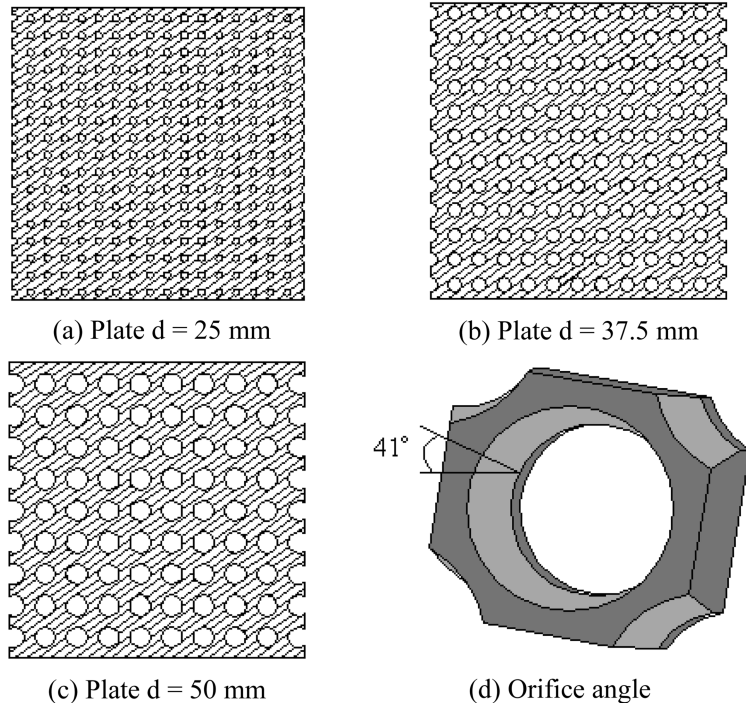


Fig. 3 The orifice perforated plate

composed of a Dantec 55P61 X-type hot-wire probe with two Dantec Streamline 55C90 hot-wire anemometer (CTA) modules, a temperature probe, an A/D converter, a light-duty 2-D traversing system and a computer, was used. The instantaneous flow velocity in the streamwise direction was measured by the X-probe. The traverse system was secured at the desired locations downstream of the orifice perforated plate along the wind tunnel center line for supporting the hot-wire probe and the temperature probe. Previous study (Liu and Ting 2007) showed that the turbulence generated by the orifice perforated plate remained non-isotropic until the wake-jet interactions mingled over a distance of approximately $10d$ downstream of the plate, where d was the diameter of the holes of the orifice perforated plate. Thus, all hot-wire data in the current study were collected at or beyond $10d$ downstream of the orifice perforated plate.

The measurement was taken over a period of 125 seconds at a sampling frequency of 80 kHz, resulting in 10,000,000 samples at each measurement location. The sampling number was chosen based on sensitivity analysis which would ensure stable and accurate mean velocity, turbulence velocity and integral length scale deductions. The collected data were low-passed at 30 kHz to avoid the aliasing problem before further analysis. A Pitot-static tube was employed at the beginning of the tests when adjusting the wind tunnel power supply to provide the desirable wind speed. It was removed during hot-wire and drag measurements.

2.2 Sphere setup

Six wood spheres with diameters D of 20, 51, 65, 102, 140 and 210 mm were used in the present study to cover a Reynolds number range of 2.2×10^4 to 8×10^4 , and to enable the independent

control of relative integral length scale Λ/D varying from 0.043 to 3.24. The surface of all the spheres were polished and waxed. The surface roughness was measured by the R_a method in material science (Czichos *et al.* 2006). The mean surface roughness was $17 \mu\text{m}$, giving a relative roughness (surface roughness/sphere diameter) of no more than 8.5×10^{-4} for the smallest sphere utilized. In other words, based on the mean surface roughness, the spheres were both mechanically and hydraulically smooth.

To minimize the influence of sphere support on the results, 0.5 mm diameter high strength polymer strings (SF24G-150 model of the FUSION® brand) with a maximum tensile capacity of 10.9 kg were used to secure the sphere in position. Two holes of 5 mm in diameter and 20 mm in depth (except for the smallest sphere, which had a depth of 9 mm) were threaded into the top and bottom side of each sphere, allowing the fastening of the supporting strings via two screws. The holes were filled with Epoxy once the screws were tightened.

A total of eight strings were utilized in the sphere setup, four of which were fastened to the top hole and another four to the bottom one, as schematically illustrated in Fig. 4. The other end of the top strings were laid symmetrically and fastened firmly to the two wind tunnel side walls with each making an angle of $[90^\circ - (\alpha \pm 0.3^\circ)]$ with respect to the test section ceiling and $\beta \pm 0.3^\circ$ to the streamwise direction of the wind tunnel. For the four bottom strings, their other ends were secured firmly to the tunnel floor, making an angle of $[90^\circ - (\alpha' \pm 0.3^\circ)]$ with respect to the test section floor and $\beta \pm 0.3^\circ$ to the streamwise direction of the wind tunnel. The string setup angles, which varied depending on the sphere size, are listed in Table 1.

2.3 Drag measurement

To measure the drag force on a sphere, a load cell (model ELG-V-1N-L03M ENTRAN) was employed to quantify the net force in the strings. It was connected to a model MROJHHS Electro-Numerics amplifier which provided a 10 V excitation to the load cell. Due to the high strength of the strings and the sphere supporting mechanisms designed for the current tests, vibration of sphere induced by wind was minimal. When the sphere was subjected to wind, only the four upstream strings, two at the top and two at the bottom, would resist the drag force on the sphere. In a typical test with specified wind velocity and turbulence level, the load cell was attached to one of the top upstream strings and one of the bottom upstream strings to quantify the net load within these two strings. Due to the symmetric layout of the strings, the drag of the sphere was therefore deduced from two times the sum of the horizontal streamwise components of the net loads in these two strings. The following equations were used to calculate the drag force:

Streamwise net component in one top string

$$F_{D_Top} = \sin\alpha \cos\beta \times F_{top} \quad (1)$$

Streamwise net component in one bottom string

$$F_{D_Bottom} = \sin\alpha' \cos\beta' \times F_{bottom} \quad (2)$$

Total drag force on the sphere

$$F_D = 2(F_{D_Top} + F_{D_Bottom}) \quad (3)$$

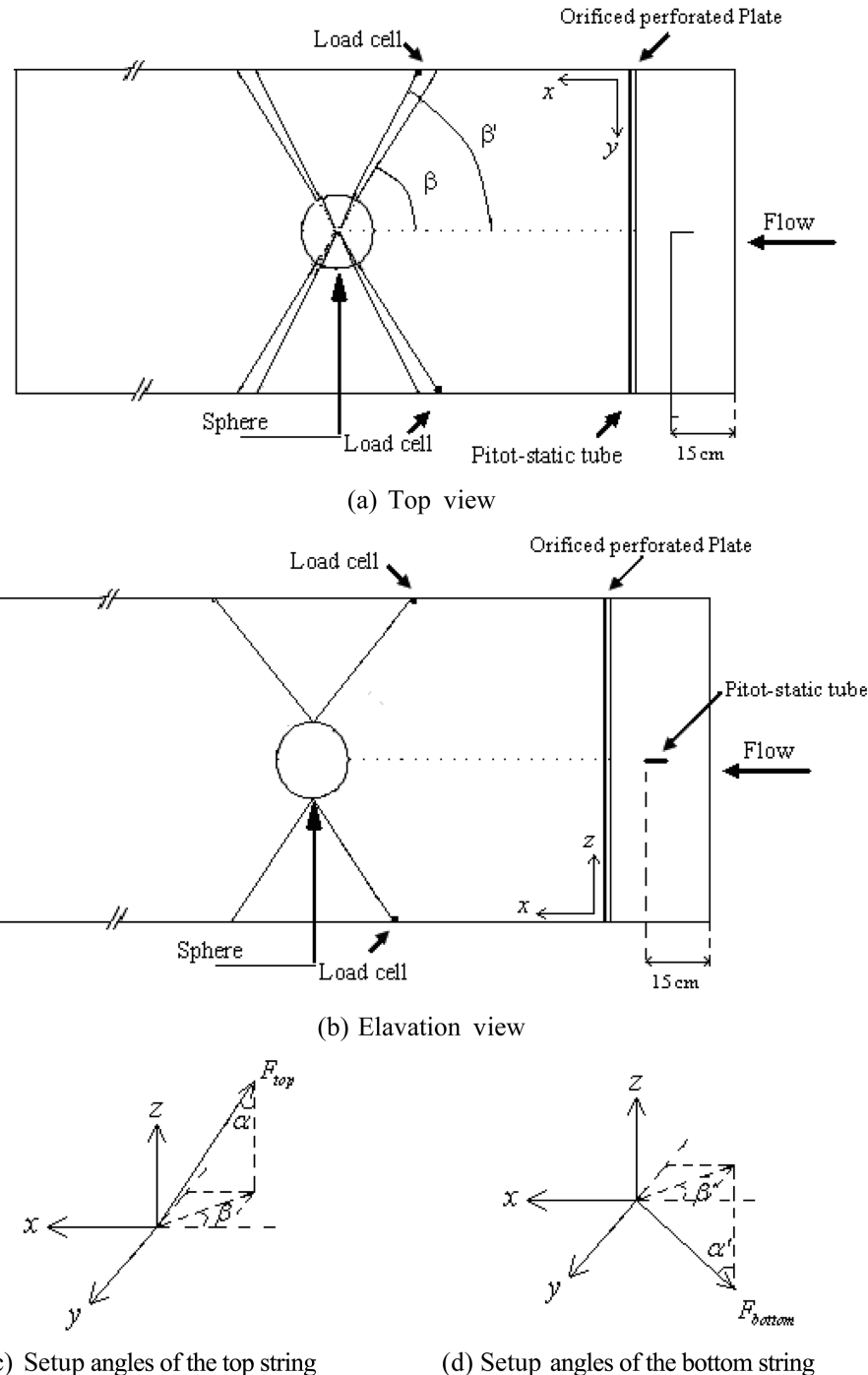


Fig. 4 Schematic of the experimental setup

In the present study, at each studied Reynolds number between 2.2×10^4 and 8×10^4 , the proper combination of orifice perforated plate hole diameter, sphere size and sphere location allowed the

Table 1 String angle in the sphere setup

Sphere type	Diameter of sphere, D (mm)	α	α'	β	β'
Wood sphere	20	53.6°	49.8°		
	51	54.9°	51.2°		
	65	55.4°	51.8°		
	102	57.0°	53.4°	37.2°	40.9°
	140	58.7°	55.2°		
	210	62.0°	58.7°		
PVC sphere [Moradian <i>et al.</i> 2009]	20, 51 and 102	40.4°	45.2°	63.5°	59.7°

quasi-independent variations of turbulence intensity and relative integral length scale from 2.5 to 6.3% and from 0.043 to 3.24, respectively.

3. Results and discussion

In this series of wind tunnel tests, the investigation on the independent effects of Reynolds number Re , turbulence intensity Tu , and relative integral length scale Λ/D on sphere drag was limited by the three available orifice perforated plates, the range of freestream velocity that the wind tunnel could provide, and the length of the test section over which the turbulence was nearly isotropic and significant. However, efforts were made to identify appropriate combinations of orifice perforated plate, the sphere location downstream of the plate and the wind tunnel speed, under which at least three data points could be obtained to isolate the impact of different turbulent flow parameters on the drag. To compare with the ‘no turbulence’ freestream flow scenario, measurements were also taken in the absence of the orifice perforated plate, i.e., in “smooth flow” where the freestream turbulence was less than 0.3%.

3.1 Turbulence parameters

Integral length scale and turbulence intensity are two important parameters for describing turbulent flow. The magnitude of integral length scale is largely dependent on the size of the holes of the orifice perforated plate and also on the spacing between adjacent holes. The approach adopted in this study is based on the Taylor’s frozen turbulence hypothesis (Taylor 1938), where Λ is defined as the product of the local time-averaged velocity \bar{U} and the time scale estimated from the autocorrelation coefficients of the instantaneous turbulence fluctuation velocity u . According to Batchelor (1967), this hypothesis is valid for turbulence intensity up to 15%. The maximum turbulence intensity achieved in this study was less than 7% and thus, the integral scale estimation is expected to be reliable. Relative turbulence intensity represents the turbulence level of flow. It is defined as the ratio of the root-mean-square velocity u_{rms} with respect to the time-averaged flow velocity \bar{U} at a specific location under consideration.

The quasi-isotropic turbulence downstream of Plate d-37.5 at 10.5 m/s has been detailed in Liu *et al.* (2007). The turbulence generated by the orifice perforated plate was found to be homogeneous over the cross section normal to the mean flow direction with Gaussian-like turbulence fluctuation.

The isotropy of the turbulence field has been portrayed by a streamwise/lateral turbulence intensity ratio of approximately 1.1. The turbulence kinetic energy decays in a power law manner as

$$\frac{u^2}{U^2} = A \left(\frac{X}{M} - \frac{X_0}{M} \right)^{-n} \quad (4)$$

with the exponent n of 1.012, implying a self-preserving state of the orifice perforated plate turbulence. Here, X is the streamwise distance downstream of the plate, X_0 is the virtual origin, M is the mesh size, A is the decay power law coefficient and n is the decay power exponent ($n = 1$ for completely self-preserving isotropic turbulence). The exponent n from the current experimental work varies between 1.02 and 1.09, depending on the plate and freestream velocity. It agrees favorably with that of Liu *et al.* (2007) and also with the analytical value derived by Speziale and Bernard (1992).

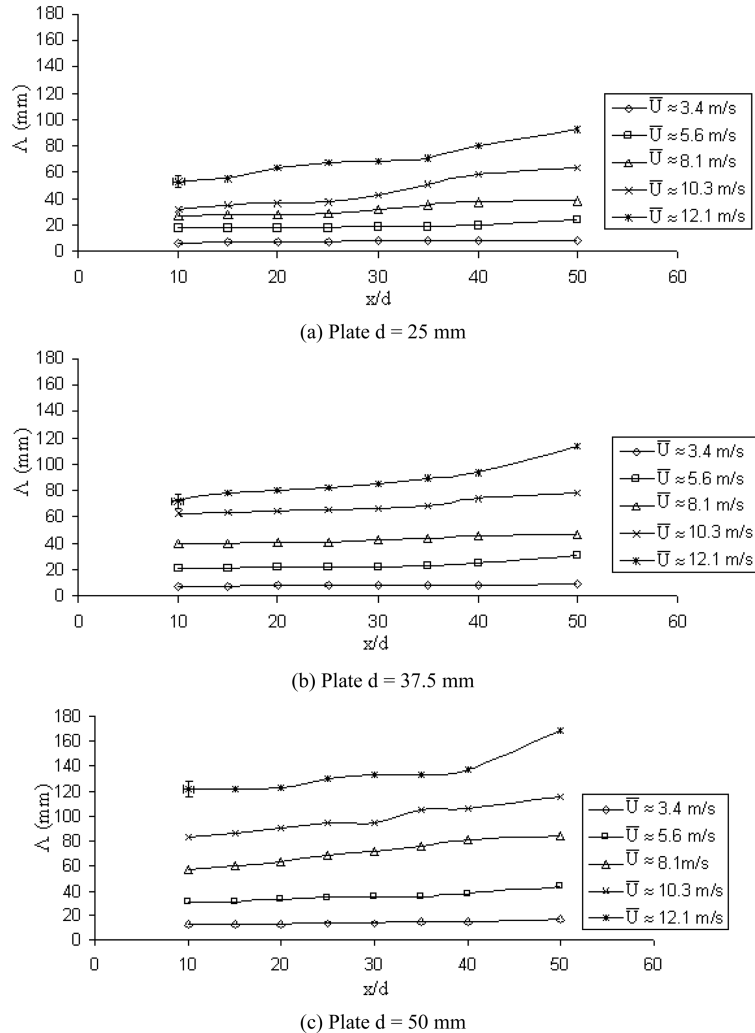


Fig. 5 Variation of integral length scale downstream of the perforated plate

Fig. 5 portrays the variation of integral length scale along the centerline of the wind tunnel with the normalized distance downstream of the plate. It is clear from this figure that the integral length scale is larger at higher wind speed, over the range of wind speed from 3.4 m/s to 12.1 m/s considered. Also, the integral length scale increases along the downstream direction. This phenomenon is more obvious when the wind speed is higher. The main source of uncertainty in the velocity measurement (the hot-wire measurement) came from its calibration. This includes the uncertainty in the reference velocity, the uncertainty in voltage reading, and the uncertainty associated with curve-fitting. The maximum uncertainties in \bar{U} and u_{rms} are estimated to be 1.2% and 2%, respectively, while their average uncertainties are estimated to be 1.1% and 1.7%, respectively. The maximum and average uncertainties of the integral length scale are estimated to be approximately 4.2% and 3.6%, respectively.

Fig. 6 depicts the variation of the turbulence intensity downstream of the orifice perforated plate at the five tested wind speeds. Results show the expected power law decay of turbulence with

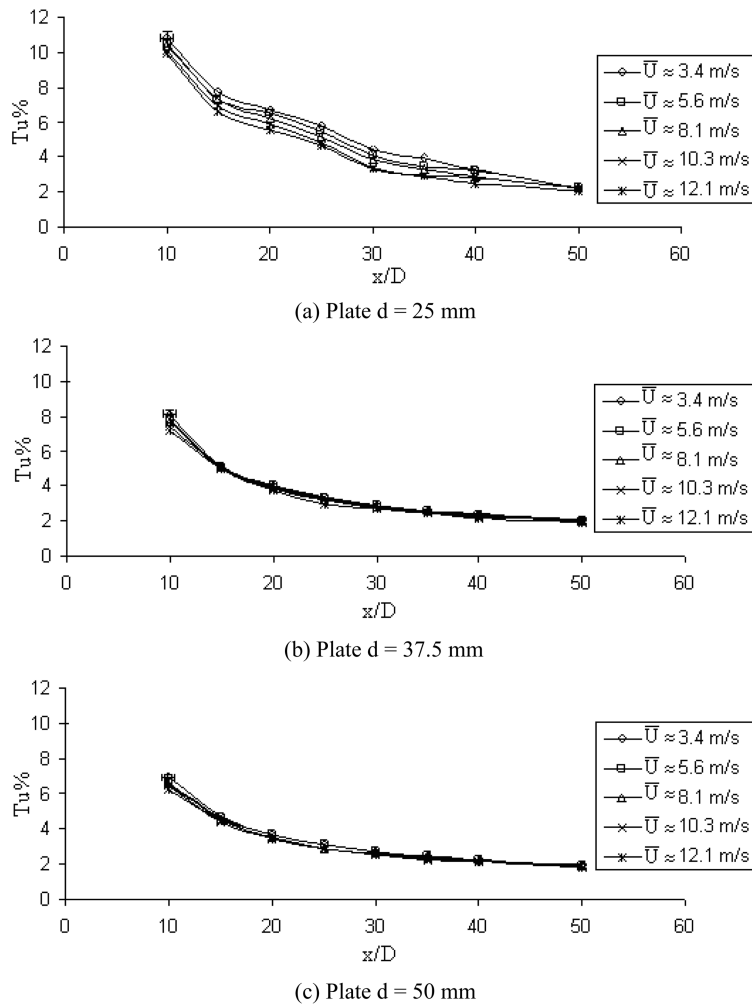


Fig. 6 Variation of turbulence intensity downstream of the perforated plate

distance downstream of the turbulence generator, as described by Eq. (4). In addition, the turbulence intensity at any given location downstream of Plate d-37.5 and Plate d-50 is insensitive to changes in freestream velocity; see Figs. 6(b) and 6(c). This invariance is not quite achieved when using Plate d-25 (Fig. 6(a)), probably because the small holes resulted in some unstable jet-wake interactions which continue relatively far downstream of the plate and thus, changes in these jet-wake intensity lead to some variations in T_u . The maximum and average uncertainties of the turbulence intensity are estimated to be approximately 2.4% and 2%. It is worth mentioning that the results in Figs. 5 and 6 are consistent with those obtained by Liu *et al.* (2007), where the same turbulence generation system was employed.

3.2 C_D - Re relation under “smooth flow” condition

The background turbulence in the absence of orifice perforated plate was found to be less than 0.3%. This level is quite typical in low-speed wind tunnels and hence, the measured drag is expected to be close to the standard curve in Fig. 1. Fig. 7 presents a comparison among the C_D - Re relation obtained in this study, that in our earlier study (Moradian *et al.* 2009) and the standard curve. The band of the standard curve is based on data from Shepherd and Lapple (1940), Torobin and Gauvin (1959), Clift and Gauvin (1970, 1971), Achenbach (1972) and Schlichting (1979). The uncertainty in the drag measurement came from four different sources - the sphere diameter measurement, the velocity measurement, the air density deduction, and the load cell measurement. The maximum and average uncertainties of sphere diameter measurement are 4% and 1.8%, respectively. The uncertainties in time-averaged velocity, sphere diameter and air density lead to average and maximum uncertainties of 2.1% and 4.2%, respectively, in Re . The maximum uncertainties in the drag coefficient of approximately 10.0% occurred when using the smallest sphere at the lowest tested velocity; the typical uncertainties are around 7.8%. Fig. 7 shows that the values of drag coefficient obtained in the current study fall within the band of the standard curve. A

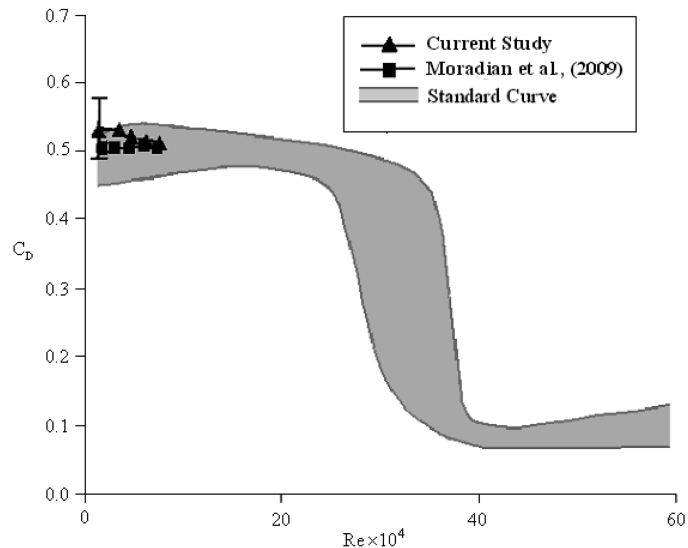


Fig. 7 Drag coefficient versus Reynolds number in smooth flow

small discrepancy between the current set of data and those by Moradian *et al.* (2009) can be observed at lower Reynolds numbers. This is probably caused by the difference in surface roughness. The smoother PVC spheres used in Moradian *et al.* (2009) have a mean roughness of 0.97; that is, less than 6% of that associated with the wood spheres used in this study. While all spheres considered in this and our previous studies can be considered hydraulically smooth (Moradian 2008), the smallest wood sphere used which gives the lowest Re data has the largest relative roughness. It is possible that some part of the surface of this smallest wood sphere could have slightly exceeded the roughness threshold which defines the sphere to be smooth.

3.3 C_D -Re relation in turbulent flow

It is known that the drag coefficient of a sphere undergoes a sudden drop at the critical Reynolds number which is approximately 3.5×10^5 under negligible turbulence condition. However, this value can be significantly altered in the presence of turbulence. To explore the impact of different turbulence parameters on the sphere drag and to identify the corresponding critical Reynolds number, drag measurement was conducted on six wood spheres for $2.2 \times 10^4 \leq Re \leq 8 \times 10^4$, Tu up to 6.3%, and $0.043 \leq \Lambda/D \leq 3.24$. The variation of C_D with respect to Reynolds number under different turbulent flow conditions are plotted in Figs. 8 and 9.

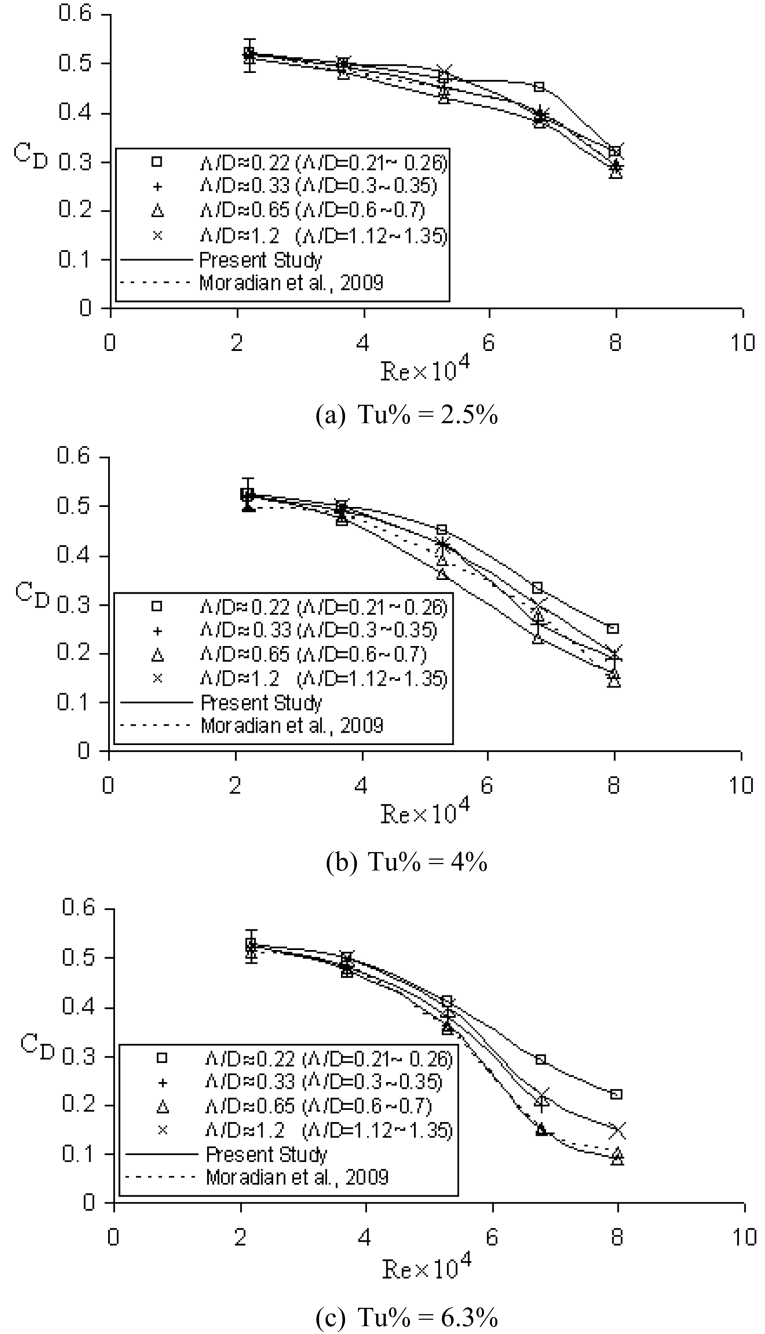
The three subplots in Fig. 8 describe the C_D -Re relation at turbulence level of 2.5%, 4% and 6.3%, respectively. Every curve in each figure corresponds to a certain relative integral length scale. The general trend of decreasing C_D with increasing Re is obvious. The detail C_D -Re pattern, on the other hand, highly depends on the turbulence level and the relative size of the eddying motion (integral length).

By comparing Figs. 8(a), 8(b) and 8(c), it can be concluded that at any particular Re and Λ/D , the drag coefficient C_D is smaller in higher turbulent wind. This is more obvious at higher Reynolds number. Also shown in Fig. 8 are the data from the three PVC spheres obtained by Moradian *et al.* (2009); these results are in excellent agreement with the current set of results based on six wood spheres.

When taking a closer look at Figs. 8(a), 8(b) and 8(c), it can be seen that among the turbulence conditions ($Tu = 2.5\%, 4\%, 6.3\%$) considered here, C_D consistently reaches its minimum when Λ/D is around 0.65. In other words, the value of C_D decreases with increasing Λ/D up to 0.65, and then it starts to increase with further increase in Λ/D beyond 0.65; the values of C_D at Λ/D of 1.2 are approximately equal to those at Λ/D of 0.33. In short, for the range of relative integral length scale investigated in this study, an eddy/sphere size ratio of approximately 0.65 appears to be most effective for lowering C_D .

Furthermore, it is observed from Fig. 8 that for Reynolds numbers less than 3.7×10^4 , C_D is relatively insensitive to changes in eddy size and turbulence intensity. The influences of the relative integral length scale and turbulence intensity become progressively more pronounced at higher Reynolds numbers. Also, the drag coefficient is most sensitive to relative integral length scale at high Tu when Λ/D is around 0.65. For example, for the $Tu \approx 6.3\%$ and $Re = 8 \times 10^4$ case shown in Fig. 8(c), when the relative integral length scale is increased from 0.22 to 0.65, the drag coefficient decreases by more than 55%, from 0.225 to 0.1; whereas when Λ/D increases from 0.65 to 1.2, C_D jumps up by 50%, from 0.1 to 0.15.

The data presented in Fig. 8 are reorganized in Fig. 9, to better reflect the effect of turbulence intensity on sphere drag. Each subplot in Fig. 9 shows the C_D -Re relation at a particular relative

Fig. 8 Variation of C_D with Re at constant turbulence intensity

integral length scale, and every curve in the figure corresponds to a certain turbulence level. In general, for all the three turbulence intensity levels studied, the drag coefficient is observed to decrease with increasing Reynolds number, for any Λ/D condition. More importantly, the $\Lambda/D=0.65$

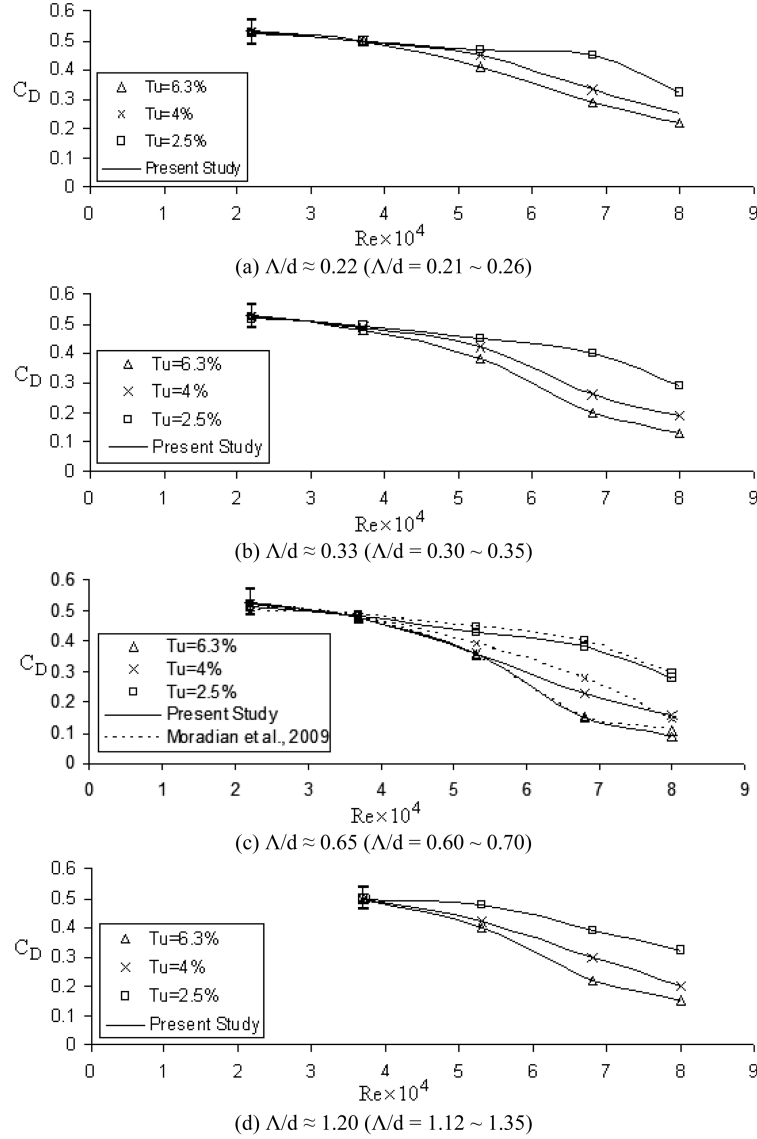


Fig. 9 Variation of C_D with Re at constant relative integral length scale

condition always leads to the lowest C_D for the same turbulence level, at any Reynolds number.

The general results of decreasing C_D with increasing Tu presented in Fig. 9 are in good agreement with those in the literature (for example, Dryden *et al.* 1937, Torobin and Gauvin 1959, Clift and Gauvin 1970), which suggest that the increase of turbulence intensity tends to advance the critical Reynolds number as a result of movement of the separation point farther downstream of the sphere. If we follow Torobin and Gauvin (1959) and define Re_{cr} as the Reynolds number at which the value of C_D is less than or equal to 0.1, then this critical condition has not been reached under most of the conditions plotted in Fig. 9. Nonetheless, the C_D corresponding to the higher turbulence level cases all tend toward this critical value. The $\Lambda/D = 0.65$ case at $Tu = 6.3\%$ in Fig. 9(c) indicates that this

critical condition has been achieved at $\text{Re} = 8 \times 10^4$, which is significantly lower than the standard smooth flow Re_{cr} of 3.5×10^5 .

Looking closer at the results documented in the literature (Figs. 1 and 2), it is found that under similar turbulent flow conditions, the critical Reynolds number values identified by Dryden *et al.* (1937), Clift and Gauvin (1970) and Moradian *et al.* (2009) agree well with that obtained in this study. As can be observed from Fig. 1, Dryden *et al.* (1937) found from their drag measurement of a fixed sphere that at turbulence intensity of 4.5%, Re_{cr} was around 9×10^4 ; whereas the numerical simulation by Clift and Gauvin (1970) showed a critical Reynolds number of 7×10^4 at Tu of 5%. Moradian *et al.* (2009) conducted drag measurement on three PVC spheres in turbulent wind, and reported that at $\text{Tu} = 6.3\%$, Re_{cr} was 8×10^4 . The small discrepancy in the quantitative results is believed to be not only induced by the slight difference in the turbulence intensity, but also some variation in Λ/D .

3.4 Combined effect of turbulence parameters on C_D

As pointed out earlier, turbulent flow has a complicated multi-aspect nature, of which the flow parameters such as turbulence intensity and integral length scale are dependent on each other. To better grasp how sphere drag would be affected by the presence of turbulence in the oncoming flow, the C_D - Re relation is shown three-dimensionally in Fig. 10. The surfaces are contours of particular turbulence intensity. The fact that C_D is lowered with increasing Tu can be readily observed. The effectiveness of this reduction is enhanced at higher Reynolds number. More interestingly, all C_D contours dip at $\Lambda/D \approx 0.65$, where the minimum C_D occurs.

Fig. 11 shows the results achieved by Neve (1986), Neve and Shansonga (1989) and the comparison between them and current results. As shown in Fig. 11(a), for their fixed sphere in turbulent freestream with $\text{Tu} = 10\%$ the effect of Λ/D is inconclusive. Even though freestream turbulence with Λ/D of 1.5 seems to significantly lower the drag coefficient for $\text{Re} < 2 \times 10^4$, this Λ/D effect diminishes at higher Re . At a higher Tu of 16% (Fig. 11(b)), on the other hand, a

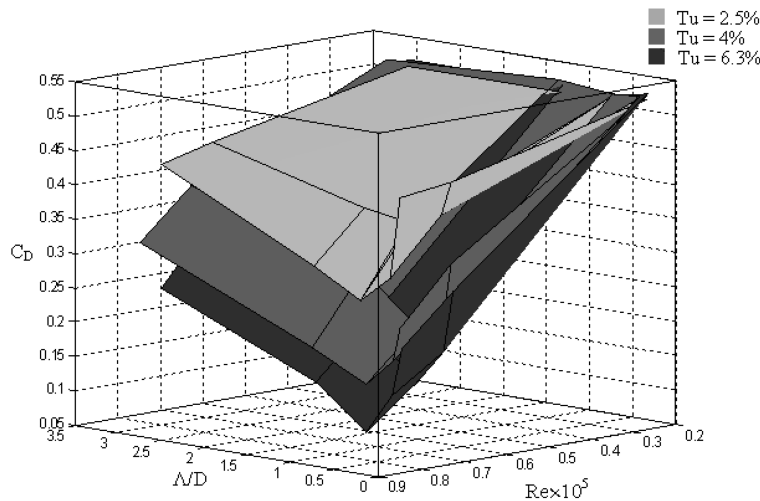
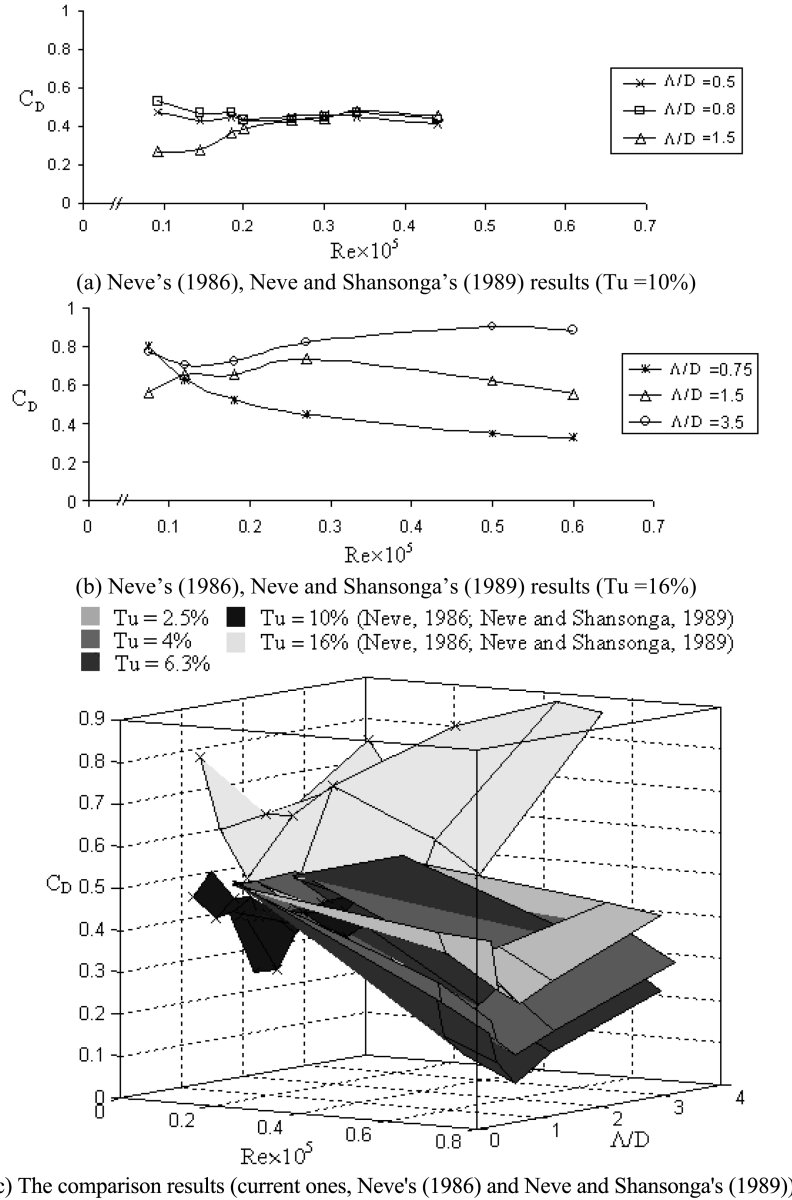


Fig. 10 Variation of drag coefficient with Re , Tu and Λ/D

Fig. 11 A comparison $C_D = f(Re, Tu \text{ and } \Lambda/D)$

smaller integral length Λ/D of approximately 0.75 leads to appreciably lower C_D , and that freestream turbulence with Λ/D of 3.5 results in relatively larger C_D for $Re > 1.2 \times 10^4$. In short, Neve and Shansonga did not reach any definite conclusion regarding the role of Λ/D . The results obtained in this study (see Fig. 11(c)), on the other hand, portray a clear trend of reduced C_D at Λ/D of about 0.65.

Physically, an increase in flow turbulence advances the boundary layer transition into a turbulent boundary at a lower Reynolds number compared to its ‘smooth flow’ counterpart. This reduces the

unfavorable pressure gradient around the sphere and hence, moves the separation point farther downstream. Consequently, the pressure drag is progressively lowered with increasing freestream turbulence. The underlying physics played by the (relative) integral length is less known. Intuitively, there are probably two key dimensions associated with a flow over a sphere. One of these is the thickness of the boundary layer, especially that just upstream of the separation point. The larger dimension is defined by the size of the wake, which can be approximated by the diameter of sphere. The results obtained in this study seem to suggest that, over the range of conditions considered here, turbulent flow with eddy sizes falling in between the small dimension of the boundary layer and the large dimension defined by the wake is most effective in advancing the drag crisis. In other words, an integral length of about 65% the diameter of the sphere appears to be most effective in perturbing the boundary layer from laminar to turbulent, and in decreasing the size of the (near) wake.

Nonetheless, it is possible for the optimum value of Λ/D , which corresponds to the lowest C_D , to deviate from 0.65 at other (higher) turbulence conditions. It is also plausible to have more than one C_D minimum, especially at very high turbulence levels. While not achieved in this study, the results obtained by researchers such as Torobin and Gauvin (1960) as shown in Fig. 1 appears to indicate the possibility to have a sunken saddle prior to the occurrence of the advanced drag crisis at higher Re . If this is truly the case, it is likely that the corresponding optimal Λ/D values for the sunken saddle and that associated with the advanced drag crisis are different.

4. Conclusions

This paper presents an experimental study on advancing the drag crisis of a sphere via the manipulation of turbulent integral scale. Six wood spheres were tested in a closed-loop wind tunnel for $2.2 \times 10^4 \leq Re \leq 8 \times 10^4$. Turbulence was generated by orifice perforated plates with turbulence intensity up to 6.3% and relative integral length scale Λ/D from 0.043 to 3.24. The variations of sphere drag with respect to Reynolds number under different turbulence conditions, were obtained and compared with that in negligible turbulence condition. It has been confirmed that the drag coefficient can be decreased and the critical Reynolds number can be advanced by increasing the flow stream turbulence intensity. More interestingly, the unique role of the relative integral length scale has been revealed. At any studied Reynolds number, the optimum size of integral length scale on lowering drag with increasing Tu is found to be about 65% the sphere diameter. In other words, decreasing Λ/D down to 0.65 increases the effect of Tu on reducing drag, while reducing Λ/D below 0.65 would lessen the influence of Tu .

Acknowledgments

The project was made possible through the financial support from Natural Sciences and Engineering Research Council of Canada (NSERC).

References

- Achenbach, E. (1972), "Experiments on the flow past spheres at very high Reynolds numbers", *J. Fluid Mech.*,

- 54(3), 565-575.
- Ahlborn, F. (1931), "Turbulence and mechanism of resistance to flow by spheres and cylinders", *J. Tech. Phys.*, **12**(10), 482-488.
- Anderson, T.J. and Uhlherr, P.H.T. (1977), "The influence of stream turbulence on the drag of freely entrained spheres", *Proceedings of the 6th Australasian Hydraulics and Fluid Mechanics Conference*, Adelaide, SA, Australia, December.
- Bakic, V. and Peric, M. (2005), "Visualization of flow around sphere for Reynolds numbers between 22000 and 400000", *Thermophys. Aeromech.*, **12**(3), 307-315.
- Batchelor, G.K. (1967), *An Introduction to Fluid Dynamics*, Cambridge University Press, USA.
- Brownlee, K.A. (1960), *Statistical Theory and Methodology in Science and Engineering*, John Wiley, New York.
- Çengel, Y.A. and Cimbala, J.M. (2006), *Fluid Mechanics: Fundamentals and Applications*, McGraw-Hill Science.
- Clamen, A. and Gauvin, W.H. (1969), "Effects of turbulence on the drag coefficients of spheres in a supercritical flow regime", *AICHE J.*, **15**(2), 184-189.
- Clift, R. and Gauvin, W.H. (1970), "The motion of particles in turbulent gas streams", *Proceedings of the Chemeca '70: A Conference convened by the Australian National Committee of the Institution of Chemical Engineers and the Australian Academy of Science*, Melbourne and Sydney, Australia, August.
- Clift, R. and Gauvin, W.H. (1971), "Motion of entrained particles in gas streams", *Can. J. Chem. Eng.*, **49**(4), 439-448.
- Czichos, H., Saito, T. and Smith, L. (2006), *Springer Handbook of Materials Measurement Methods*, Springer Berlin Heidelberg.
- Dryden, H.L. and Kuethe, A.M. (1930), *Effect of turbulence in wind tunnel measurements*, National Advisory Committee for Aeronautics, Report No. 342.
- Dryden, H.L., Schubauer, G.B., Mock, W.C. and Bkrambtad, H.K. (1937), *Measurements of intensity and scale of wind-tunnel turbulence and their relation to the critical Reynolds number of spheres*, National Advisory Committee for Aeronautics, Report No. 581.
- Lamb, H. (1945), *Hydrodynamics*, 6th Ed., Dover Publications, New York.
- Liu, R. and Ting, D.S.K. (2007), "Turbulent flow downstream of a perforated plate: Sharp-edged orifice versus finite-thickness holes", *J. Fluid. Eng.-T. ASME*, **129**(9), 1164-1171.
- Liu, R., Ting, D.S.K. and Checkel, M.D. (2007), "Constant Reynolds number turbulence downstream of an orificed, perforated plate", *Exp. Therm. Fluid Sci.*, **31**(8), 897-908.
- Mohd-Yusof, J. (1996), *Interaction of massive particles with turbulence*, PhD Thesis, Department of Mechanical Engineering, Cornell University.
- Moradian, N. (2008), *The effects of freestream turbulence on the drag of a sphere*, MASc Thesis, University of Windsor.
- Moradian, N., Ting, D.S.K. and Cheng, S. (2009), "The effects of freestream turbulence on the drag coefficient of a sphere", *Exp. Therm. Fluid Sci.*, **33**(3), 460-471.
- Neve, R.S. (1986), "The importance of turbulence macroscale in determining the drag coefficient of spheres", *Int. J. Heat Fluid Fl.*, **7**(1), 28-36.
- Neve, R.S. and Shansonga, T. (1989), "The effects of turbulence characteristics on sphere drag", *Int. J. Heat Fluid Fl.*, **10**(4), 318-321.
- Prandtl, L. (1914), *Der luftwiderstand von kugeln*, Nachrichten von der Königliche Gesellschaft der Wissenschaften zu Göttingen, Mathematisch-Physikalische Klasse, 177-190.
- Sankagiri, S. and Ruff, G.A. (1997), "Measurement of sphere drag in high turbulent intensity flows", *Proceedings of the ASME Fluids Engineering Division Summer Meeting (FEDSM'97)*, Vancouver, Canada, June.
- Schlichting, H. (1955), "Berechnung der reibungslosen, inkompressiblen Strömung für ein vorgegebenes ebenes Schaufelgitter", *Verein Deutscher Ingenieure -- VDI Zeitschrift*, No. 447, 269-270.
- Schlichting, H. (1979), *Boundary Layer Theory*, McGraw-Hill.
- Shepherd, C.B. and Lapple, C.E. (1940), "Flow pattern and pressure drop in cyclone dust collectors", *J. Ind. Eng. Chem.*, **32**, 1246-1248.
- Speziale, C.G. and Bernard, P.S. (1992), "The energy decay in self-preserving isotropic turbulence revisited", *J. Fluid Mech.*, **241**, 645-667.

- Taylor, G.I. (1938), "The spectrum of turbulence", *Proc. Roy. Soc. A-Math Phys.*, **164**, 476-490.
 Torobin, L.B. and Gauvin, W.H. (1959), "Fundamental aspects of solids-gas flow, Part II: the sphere wake in steady laminar fluids", *Can. J. Chem. Eng.*, **37**, 167-176.
 Torobin, L.B. and Gauvin, W.H. (1960), "Fundamental aspects of solids-gas flow, Part V: the effects of fluid turbulence on the particle drag coefficient", *Can. J. Chem. Eng.*, **38**, 189-200.
 Torobin, L.B. and Gauvin, W.H. (1961), "The drag coefficients of single spheres moving in a steady and accelerated motion in a turbulent fluid", *AICHE J.*, **7**(4), 615-619.
 Zarin, N.A. (1970), *Measurement of non-continuum and turbulence effects on subsonic sphere drag*, NASA Report, NCR-1585.
 Zarin, N.A. and Nicholls, J.A. (1971), "Sphere drag in solid rocket--non-continuum and turbulence effects", *Combust. Sci. Technol.*, **3**(6), 273-285.

CC

Nomenclature

A	decay power coefficient
C_D	drag coefficient
D	diameter of spheres (m)
d	diameter of holes of the orifice perforated plates (m)
F_{bottom}	net force in a bottom string (N)
F_{D_Bottom}	streamwise net component in a bottom string (N)
F_{D_Top}	streamwise net component in a top string (N)
F_{top}	net force in a top string (N)
M	mesh size
N	sampling number
n	decay power exponent
Re	Reynolds number, UD/v
Re_{cr}	critical Reynolds number
Tu	turbulence intensity, u_{rms}/\bar{U} (%)
U	mean flow velocity (m/s)
\bar{U}	time-averaged velocity (m/s)
u	instantaneous fluctuating velocity (m/s)
u_{rms}	root mean square velocity (m/s)
X	streamwise distance downstream of the plate
X_o	virtual origin

Greek Symbols

Λ	integral length scale (m)
$\alpha, \alpha', \beta, \beta'$	angles associated with sphere attachment with respect to the walls (deg)